https://doi.org/10.15407/knit2022.05.015
UDC 629.78

M. O. REDKA, PhD student
E-mail: mix5236@ukr.net
S. V. KHOROSHYLOV, Leading researcher, Dr. Sci. in Tech., Professor
ORCID.org/0000-0001-7648-4791
E-mail: skh@ukr.net

Institute of Technical Mechanics of the National Academy of Sciences of Ukraine and the State Space Agency of Ukraine
15 Leshko-Popel St., Dnipro, 49005 Ukraine

DETERMINATION OF THE FORCE IMPACT OF AN ION THRUSTER PLUME ON AN ORBITAL OBJECT VIA DEEP LEARNING

The subject of research is the process of creating a neural network model (NNM) for determining the force impact of an ion thruster (IT) plume on an orbital object during non-contact space debris removal. The work aims to develop NNMs and study the influence of various factors on the accuracy of determining the force transmitted by the ion plume of the thruster to a space debris object (SDO). The tasks to resolve are to choose the structures of the NNMs, form a data set and use this data to train and validate the NNMs, and to explore the influence of the model structure and optimizer parameters on the accuracy of force determination. The methods used are plasma physics, computer simulation, deep learning, and optimization using an improved version of stochastic gradient descent. As a result of research, three NNMs have been developed, which differ in the number of hidden layers and neurons in hidden layers. For training and validation of the NNMs, a data set was generated for an SDO approximated by a cylinder using an autosimilar description of the ion plasma propagation. The data set was obtained for various relative positions and orientations of the object in the process of its removal from an orbit. Using this data set, the NNM parameters were optimized with the supervised learning method. The optimizer and its parameters are selected, providing a small error at the stage of validating learning outcomes. It was found that the accuracy of determining the force depends on the relative position and orientation of the SDO, as well as the architecture of the NNM, and the features of this influence were identified. The approach applied allows us to obtain the possibility of using methods of deep learning to determine the force impact of the IT plume on the SDO. The proposed models provide the accuracy of the force impact determination, which is sufficient for solving the considered class of problems. At the same time, NNM makes it possible to obtain results much faster in comparison with the methods used previously. This fact makes the NNMs promising to use both on-board and in mathematical modeling of missions to remove space debris.

Keywords: *ion thruster, space debris object, transmitted force, neural network model, deep learning.*

INTRODUCTION

At present, there are a large number of space objects in near-Earth space, such as fragments of launch vehicle stages, non-functioning spacecrafts and their fragments, which significantly complicate further space activities [14]. In this regard, the task of creating tools and technologies for the direct removal of space debris objects (SDO) from near-Earth orbits is now urgent.

Various concepts of active debris removal are known, for example, laser systems [16], electrodynamic tether systems [18], and combined systems [7, 9]. Most concepts involve docking the removal sys-

Цитування: Redka M. O., Khoroshylov S. V. Determination of the force impact of an ion thruster plume on an orbital object via deep learning. *Space Science and Technology.* 2022. **28**, № 5 (138). P. 15—26. https://doi.org/10.15407/knit2022.05.015

tem with an SDO or capturing it with assistive devices. However, this operation can be technologically complex and unsafe.

The "Ion beam shepherd" concept was proposed for the non-contact removal of orbital objects [3]. The basic principle of this concept is to use the ion plume of an IT as a way to transmit the force impulse to the SDO for its deceleration. Such removal of space debris has a number of advantages compared to other known approaches [16, 18], namely, removal efficiency, low risk level, reusability, and technological readiness.

One of the key tasks within the concept of "Ion beam shepherd" is the determination of the force transmitted to the SDO by the shepherd. Knowledge of this force is necessary for the successful implementation of the selected removal program and can also be useful for solving problems of navigation and relative control of the "shepherd — SDO" system [2, 11, 12]. Determining this force is not an easy task since its value depends in a complex way not only on the properties of the IT plume but also on the relative position and orientation of the SDO.

A number of publications address this problem. For example, [5] proposes the theoretical foundations for modeling an ion beam plume and calculating the transmitted force. The authors of this work used an approach based on the integration of elementary forces over the surface of the object. But, as practice shows, the implementation of such a calculation method can lead to cumbersome algorithms and time-consuming modeling, so the application of these results in the form of algorithms on the shepherd board seems difficult. In [4], the possibility of an analytical description of the force is considered, however, the authors obtained such expressions only for the SDO of a spherical shape. An approach to determine the transmitted force using the central projection of the target onto a selected plane is proposed in [1, 8]. Despite the fact that this approach significantly speeds up the force calculation in comparison with the direct integration over the SDO surface, it still requires significant computational resources due to loops needed for calculating elementary forces.

At this time, artificial intelligence methods attract a significantly increased interest in the world, which is largely due to the impressive results obtained using deep learning (DL) technologies [15] — machine learning methods based on multilayer artificial neural networks (ANN). Recently, DL has been rapidly developing and demonstrating promising opportunities in solving complex problems and finding nontrivial solutions to existing problems [13, 17]. Most of the results used in practice are obtained using the methods of supervised learning or example-based learning. Despite the fact that ANN training can take a long time, the trained network allows getting results pretty fast. This feature determines the prospects of DL methods for finding the force transmitted to the SDO by the shepherd. However, it is known that the success of solving a problem by DL methods largely depends on the correct choice of the ANN structure, as well as algorithms and learning parameters. These issues are studied in this article.

The goal of the study is to develop the NNM for determining the force transmitted by an IT plume to an SDO and to investigate the influence of various factors on its accuracy.

1. PROBLEM STATEMENT

1.1. ***Reference frames.*** In the research, the following right-handed orthogonal reference frames are used. The IT-fixed reference frame (IRF) $O_I x_I y_I z_I$ has the origin O_I located at the top of an imaginary cone of the ion beam. The axis $O_I z_I$ coincides with the axis of the beam and is directed towards the thruster nozzle. It is assumed that the IT is fixed on the "shepherd", which is oriented in such a way that the axis $O_I z_I$ coincides with the tangent to the orbit and is directed to the target, the axis $O_I y_I$ coincides with the normal to the orbit and is directed in the direction opposite to the Earth, and the axis $O_I x_I$ complements the reference frame to the right-handed one.

The origin of the reference frame associated with the SDO (SDF) $O_S x_S y_S z_S$ is located at its center of mass. The direction of the SDF axes coincides with the principle inertia axes of the SDO. The orientation of the SDF axes relative to the IRF is determined by the Euler angles ϕ, ϑ, ψ [8] with z-y-x rotation sequence. The position of the origin of the SDF, relative to the IRF, is determined by the vector B_I^{SI}.

1.2. ***Model of the ion thruster plume.*** The plasma plume of an IT can be conventionally divided into near (usually less than a meter from the IT) and far

regions [5]. For the problem of contactless space debris, the far region of the plume is of primary interest since the interaction between the plasma and the target occurs within this region.

A number of mathematical models have been proposed to describe the far region of the IT plume, which differ in complexity and accuracy [5]. In this case, the so-called self-similar model of plasma propagation can be chosen as a compromise.

Self-similar models are based on the assumption that the nature of ion propagation can be described using a dimensionless similarity function as follows

$$r(z) = r_0 h(\tilde{z}),\ \tilde{z} = z / R_0,$$

where r, z are the radial and axial coordinates of the ions, respectively, R_0, r_0 are the beam radius and radial coordinates of ions at the beginning of the far region ($z = 0$).

Using the function $h(\tilde{z})$, the plasma density at an arbitrary point with coordinates r, z, can be determined as follows [12]:

$$n = \frac{n_0}{h^2(\tilde{z})} \exp\left(-C\frac{\tilde{r}^2}{2h^2(\tilde{z})}\right),$$

$$\tilde{r} = r / R_0, \qquad (1)$$

where n_0 is the plasma density at the beginning of the far region of the beam, C is the factor that determines how much of the plasma plume hit a circle of radius R_0 (for example, corresponds to 95 % of the flow hit).

It should be noted that when $M_0 >> 1$, the character of the ion plasma distribution approaches a cone, although, strictly speaking, it is not. At the same time, when $M_0 \geq 40$ and the distance to the target is less than 10 meters, the character of plasma distribution can be considered conical. In this case, the similarity function can be defined in the following form

$$h = 1 + \tilde{z}\tan\alpha_0,$$

where α_0 is the initial divergence angle of the plume. The initial divergence angle is equal to half the opening angle of the cone restricting 95 % of the plasma plume. For the problem under consideration, we can assume that the axial component of the plasma ion velocity remains constant:

$$u_z = u_{z0} = \text{const}. \qquad (2)$$

The radial velocity component within the considered model is determined by the following expression [12]:

$$u_r = u_{z0} \cdot (\tilde{r} / \tilde{z}). \qquad (3)$$

1.3. ***Interaction of the ion beam with SDO.*** The IT plume is a stream of heavy ions of propellant (for example, xenon), accelerated to an energy level of several kiloelectron-volts. When such a plume affects a solid body, a force is applied to the latter, which is mainly due to the momentum of the plasma ions bombarding the target.

Neglecting the effects of plasma ions leaving the target surface, sputtering of its material, and electron pressure, the elemental force transmitted to the SDO can be calculated as follows [12]:

$$dF = mnU(-V \cdot U)ds, \qquad (4)$$

where U is the particle velocity vector, ds is the elementary area of the target surface, V is the unit normal vector to the elementary area.

The force F transmitted to the SDO by the IT plume can be calculated by integrating the elementary forces (4) over the irradiated surface S of the target

$$F = \int_S dF.$$

In the general case, this force depends on the properties of the IT, the shape and size of the SDO, as well as on its relative position and orientation. Taking into account that for a specific mission of space debris removal, the IT properties, the shape and dimensions of the SDO are known and do not change, we can design an NNM that receives the values of the relative position and orientation of the SDO as an input and outputs force projections in the IRF.

2. DESIGN AND STUDY OF NEURAL NETWORK MODELS

2.1. ***Methodology and model structure.*** An ANN is a system of interconnected artificial neurons. A multilayer neural network is an ANN consisting of input, output, and hidden layers of neurons located between them. Such networks are more capable than single-layer neural networks. It was proved in [6, 10] that neural networks with both one and several hidden layers can be used as universal approximators of continuous functions of a set of variables, and the only

Table 1. **NNM configurations**

Name	Architecture		Activation functions
	Number of hidden layers	number of neurons	
NN-512	4	6×512×256×128×64×3	ReLU
NN-1024	4	6×1024×512×256×128×3	ReLU
NN-1024-512	5	6×1024×512×256×128×64×3	ReLU

Table 2. **Results of NNM training**

NNM	Optimizer	Validation accuracy MSE, %	Training time, s
NN-512	Adam	99.26	1575
NN-1024	Adam	99.41	3123
NN-1024-512	Adam	99.43	3028

Table 3. **Coordinates of center of mass and orientation parameters of SDO. Variable parameters marked as ***

No	Coordinates of center of mass			Orientation parameters		
	b_I^x, m	b_I^y, m	b_I^z, m	ϑ, rad	ϕ, rad	ψ, rad
1	*	0	7	0	0	0
2	0	*	7	0	0	0
3	0	0	*	0	0	0
4	0	0	7	*	0	0
5	0	0	7	0	*	0
6	0	0	7	0	0	*
7	*	1	9	1.507	1.507	1.507
8	1	*	9	1.507	1.507	1.507
9	1	1	*	1.507	1.507	1.507
10	1	1	9	*	1.507	1.507
11	1	1	9	1.507	*	1.507
12	1	1	9	1.507	1.507	*
13	*	1	9	−1.507	−1.507	−1.507
14	1	*	9	−1.507	−1.507	−1.507
15	1	1	*	−1.507	−1.507	−1.507
16	1	1	9	*	−1.507	−1.507
17	1	1	9	−1.507	*	−1.507
18	1	1	9	−1.507	−1.507	*

condition is a nonlinearity of the activation function in hidden layers.

In this work, the ReLU activation function was used for all NNMs, which transforms the input signal in the following way

$$R(\tilde{x}) = \max(0, \tilde{x}).$$

The inputs of the activation functions are determined by the values of the weights (synapses) and biases. These parameters are set as a result of NNM learning using optimization algorithms. The learning goal is to minimize errors in the ANN output. Currently, the most commonly used learning algorithms are improved versions of stochastic gradient descent (SGD), such as root mean squared propagation (RMSprop) and adaptive moment estimation (Adam) methods. In this work, the Adam optimizer was used to train neural networks. The mean squared error was used as a loss function for training and validation.

To solve the problem, three different NNM configurations with fully connected layers are considered. They differ in the number of hidden layers, as well as the number of neurons in the hidden layers. NNM configurations are summarized in Table 1.

The total number of neurons in the hidden layers of the neural network NN-512 is 960, and in the hidden layers of the neural networks NN-1024 and NN-1024-512, there are 1920 and 1984 neurons, respectively.

Training, validation, and testing of NNMs, as well as data preprocessing, were carried out using Python 3.9 programming language and Keras, Scikit-learn, Numpy and Scipy libraries.

2.2. ***Initial data.*** The following IT parameters were used for the calculations: initial radius: R_0 = = 0.0805 m; ion mass (xenon) $m = 2.18 \cdot 10^{-25}$ kg; initial plasma density $n_0 = 4.13 \cdot 10^{15}$ m^{-3}; initial axial velocity of ions u_0 = 71580 m/s; divergence angle $\alpha_0 = 7$ deg; initial electron temperature $T_e = 0.001$ eV.

The upper stage of the Cyclone-3 launch vehicle is considered as the SDO, which is approximated by a cylinder with a height of h=2.6 m and a base diameter of d =2.2 m.

2.3. ***Dataset for training and validation.*** For training and validation of the NNMs, a dataset was generated that includes input values — the coordinates of

the center of mass and the angles of orientation of the SDO relative to the IRF, and the output values of the projections of the transmitted force corresponding to them. The ground truth force outputs were calculated using the methodology presented in Section 1. During dataset generation, the input data were set randomly in the range of variation of each parameter using a uniform distribution. Range of variation of input parameters: for the parameters b_I^x and b_I^y it is [−1.0...1.0]; for the parameter b_I^z it is [5.0...9.0]; for the parameters ϑ, ϕ and ψ it is [1.507...1.507]. Then the dataset was normalized to obtain values in a range of [−1.0...1.0].

The dataset, which contains 3 500 000 records, is split for training and validation with a ratio of 80 % and 20 %, respectively.

2.4. ***Training and validation.*** NNMs were trained using a personal computer with a 10th generation Intel processor, which has 8 cores and 16 threads. The Xavier method was used to initialize the NNM weights. The learning rate for each NNM was chosen as 0.0001. The mini-batch size and the number of training epochs were selected as 256 and 100, respectively. Adam optimizer is used with the following parameters: gradient damping factor is 0.9; attenuation coefficient of the squared gradient is 0.999; the small constant is $7.000 \cdot 10^{-7}$. Adam optimizer was chosen because it is computationally efficient, has little memory requirement, invariant to diagonal rescaling of gradients, and is well suited for problems that are large in terms of data/parameters.

To determine the best NNM, they were compared with each other in terms of validation accuracy and training time. Table 2 summarizes the results of NNM training. The results show that the NNM with the smallest number of neurons in the hidden layers shows a lower validation accuracy compared to other network configurations. However, it takes almost half the time for training than others. The NNMs with the largest number of neurons in the hidden layers have approximately the same training time and accuracy.

2.5. ***Testing.*** Table 3 presents the computational cases that differ in the values of the position and orientation of the SDO relative to the IRF. The parameters marked as variables took values within the considered ranges (see Table 1) with a fixed step equal to 0.001. The parameter values of the first 6 cases are nominal.

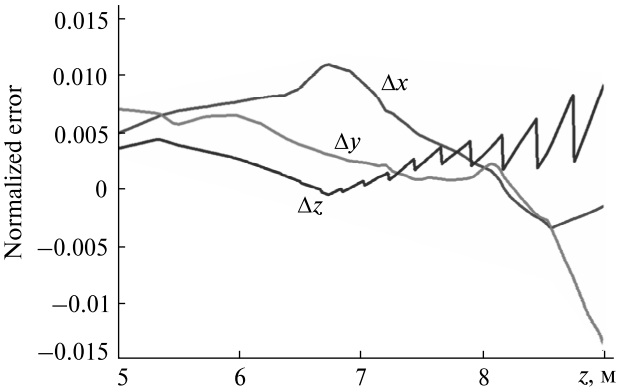

Figure 1. The values of the normalized error for each of the outputs of the NNM. Case 3 (NN-512)

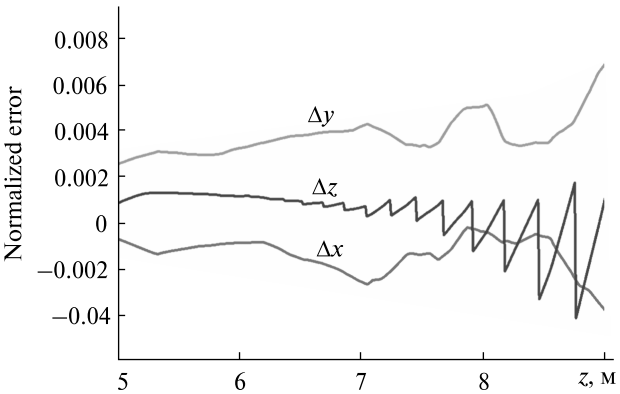

Figure 2. The same. Case 3 (NN-1024)

Pictures 1—8 show plots for normalized errors for some of the computational cases. The variable parameter is displayed along the abscissa-axis. The ordinate axis shows the values of the normalized error for each of the outputs of the NNM.

The components of the normalized error vector are defined as follows:

$$\Delta F^k = F_R^k - F_P^k, \; k = x, y, z,$$

where F_R is the normalized reference force vector, F_P is the force vector predicted by the NNM.

Figures 1—3 show the results of testing three NNM configurations for case 3.

In general, according to the figures above, it can be concluded that the accuracy of the NN-512 model is

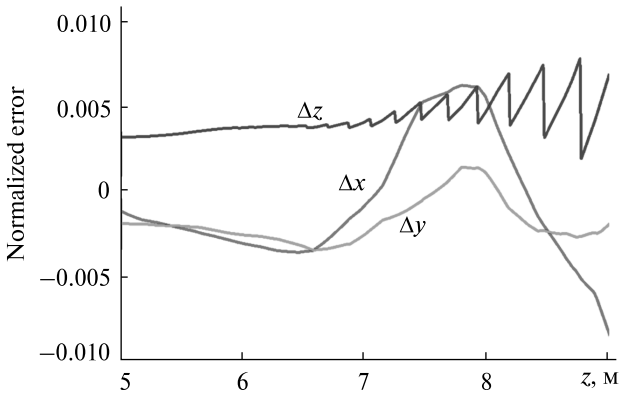

Figure 3. The same. Case 3 (NN-1024-512)

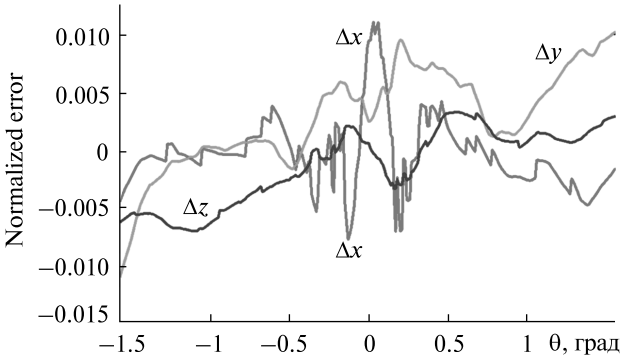

Figure 4. The same. Case 5 (NN-512)

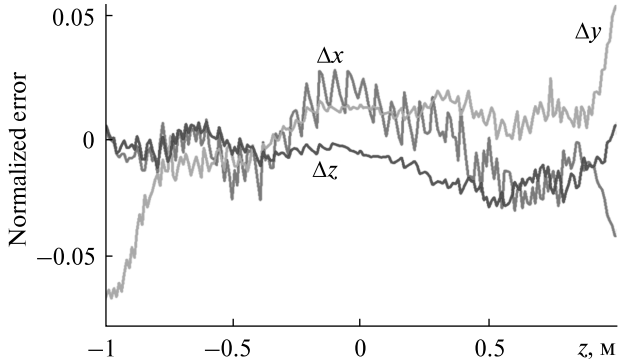

Figure 5. The same. Case 13 (NN-1024)

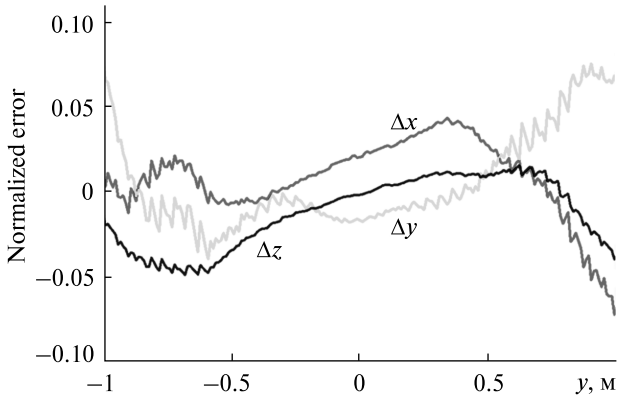

Figure 6. The same. Case 14 (NN-512)

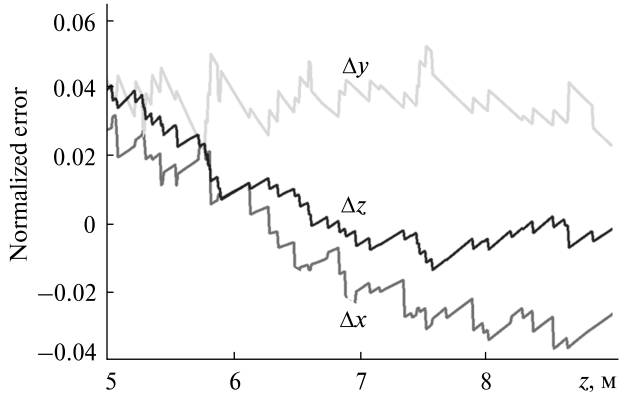

Figure 7. The same. Case 15 (NN-1024-512)

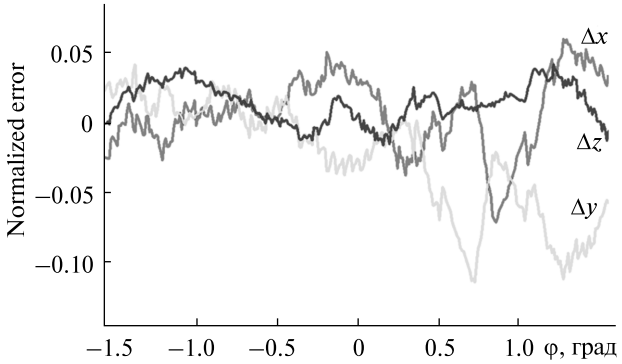

Figure 8. The same. Case 17 (NN-1024-512)

worse than that of the other two models. Figures 4—8 show the results of NNM testing for other cases.

2.6. ***Model accuracy analysis.*** To compare the results, maximum errors in determining the force transmitted to the SDO for each case from Table 5 are calculated for two intervals of variation of the input values: full and reduced (half the full).

Maximum errors in the Tables 4—9 are given for both absolute errors and errors relative to reference values.

Table 4. **Errors of force prediction for the NN-512 over the full variation interval**

No	AE			RE		
	Δf^x, 10^{-5} N	Δf^y, 10^{-5} N	Δf^z, 10^{-3} N	Δf^x, %	Δf^y, %	Δf^z, %
1	–1.7	1.6	–0.811	2.720	2.463	2.524
2	–1.4	2.5	–1.023	2.192	3.873	3.186
3	0.7	–0.9	0.303	1.098	1.367	0.944
4	0.7	0.2	0.024	1.088	0.281	0.073
5	0.6	0.7	–0.045	0.987	1.064	0.660
6	0.7	–4.2	–0.224	1.105	1.094	0.698
7	–4.1	4.7	1.183	6.425	7.329	3.685
8	–5.4	5.1	–1.477	8.432	8.041	4.600
9	–4.5	6.3	1.359	7.064	9.931	4.232
10	–4.2	4.8	–0.097	6.532	7.532	0.301
11	–9.6	5.0	1.504	14.991	7.848	4.683
12	–4.9	–7.9	–1.406	7.657	12.307	4.380
13	–4.3	4.6	–2.542	6.752	7.190	7.915
14	–4.7	4.9	–1.581	7.228	7.646	4.924
15	–5.1	4.7	2.174	7.909	7.427	6.772
16	–4.3	3.8	–1.333	6.752	6.016	4.152
17	–11.9	–8.1	1.938	18.694	12.604	6.037
18	–4.3	3.8	–1.460	6.752	6.016	4.548
Mean	4.056	3.91	1.147	6.354	6.113	3.573

Table 5. **Errors of force prediction for the NN-1024 over the full variation interval**

No	AE			RE		
	Δf^x, 10^{-5} N	Δf^y, 10^{-5} N	Δf^z, 10^{-3} N	Δf^x, %	Δf^y, %	Δf^z, %
1	1.3	0.9	–0.656	2.007	1.390	2.043
2	0.9	2.0	–0.456	1.362	3.094	1.419
3	–0.2	0.4	–0.133	0.386	0.695	0.414
4	–0.2	0.3	0.028	0.271	0.428	0.086
5	–0.5	0.7	–0.140	0.748	1.162	0.436
6	–0.6	0.6	–0.141	0.863	0.871	0.440
7	–3.3	–2.9	1.118	5.111	4.474	3.483
8	–2.0	–3.0	0.961	3.059	4.642	2.993
9	–1.8	–2.1	1.990	2.811	3.282	6.198
10	–2.1	–2.1	0.961	3.283	3.282	2.993
11	–8.2	–3.8	1.297	12.792	5.910	4.040
12	–1.9	–3.9	0.958	2.924	6.079	2.984
13	–2.7	–4.4	–0.945	4.208	6.891	2.944
14	4.7	5.0	–0.317	7.356	7.862	0.986
15	–3.2	4.3	2.211	5.048	6.779	6.886
16	–2.7	3.6	0.170	4.208	5.637	0.530
17	–4.5	–9.3	–1.040	6.971	14.599	3.240
18	–2.7	3.6	–0.383	4.208	5.588	1.194
Mean	2.0	3.0	0.770	3.756	4.593	2.406

First, let us compare the results over the full range of the input variation. Table 4 shows the maximum errors obtained using the NN-512 model. For this model, the maximum relative error (RE) of the force determination is 18.694 %, which is obtained for *X*-axis in case 17. However, the absolute error (AE) is $-1.190 \cdot 10^{-4}$ N, which is not significant. For cases where non-variable parameters have nominal values (cases 1—6), the maximum value of RE is 3.873 % (AE is $2.500 \cdot 10^{-5}$ N) and occurs at the *Y*-output for case 2.

Table 5 contains the maximum errors over the full range of the input variation for the NN-1024 model. The maximum RE is 14.599 % (AE is $-9.300 \cdot 10^{-5}$ N) and takes place at the *Y*-output for case 17. In cases 1—6, the maximum RE was observed at the Y-output for case 2 (as in the model NN-512) and is 3.094 %, which corresponds to an AE of $2.000 \cdot 10^{-5}$ N.

Table 6 summarizes the maximum errors of the model NN-1024-512 for the full range of the input variation. Here, as well as in the cases for other models, the maximum RE is 11.570 % and takes place for case 17 along the *Y*-axis, which corresponds to an AE of $-7.400 \cdot 10^{-5}$ N. For cases 1–6, the maximum RE is 2.524 % (AE is $1.600 \cdot 10^{-5}$ N) and occurs at the *X*-output for case 1.

As can be seen, case 17 is the most problematic for all NNMs, where the SDO orientation angle varies over the full variation range, and the other input parameters have non-nominal values. It can be asserted that the NN-1024-512 model provides the best result of the three model configurations, showing the smallest values of the maximum errors for all cases. The model NN-512 demonstrates the worst results.

Next, the maximum errors over a reduced variation interval are compared. Such data are presented in Tables 7—9 for models NN-512, NN-1024, and NN-1024-512, respectively. It can be seen from Table 7 that the maximum RE for the NN-512 model is 14.139 % (AE is $-9.000 \cdot 10^{-5}$ N) and is observed at the *X*-output for case 17. As for cases with nominal non-variable parameters (1—6), the worst RE is 2.81 6 % (AE $1.800 \cdot 10^{-5}$ N) and takes place at the *Y*-output for case 2.

For the NN-1024 model, the maximum RE over the reduced interval (Table 8) is 14.599 % (AE $-9.300 \cdot 10^{-5}$ N) at *Y*-output for case 17. For cases 1—6, the maximum RE is 1.488 % (AE $-9.300 \cdot 10^{-5}$ N) at *Y*-output for case 2. The data in Table 9 indicate that the maximum RE for the NN-512-1024 model is 11.570 % (AE $-7.400 \cdot 10^{-5}$ N) at

Table 6. **Errors of force prediction for the NN-1024-512 over the full variation interval**

No	AE			RE		
	Δf^x, 10^{-5} N	Δf^y, 10^{-5} N	Δf^z, 10^{-4} N	Δf^x, %	Δf^y, %	Δf^z, %
1	1.6	0.6	–6.07	2.524	1.007	1.890
2	1.3	1.3	4.83	2.076	2.009	1.503
3	–0.6	–0.2	2.49	0.882	0.346	0.777
4	–0.1	–0.2	1.37	0.080	0.267	0.427
5	–0.2	–0.6	1.33	0.388	0.921	0.415
6	0.4	–0.3	1.42	0.619	0.509	0.443
7	–3.9	–4.5	–10.58	6.145	7.018	3.295
8	–2.3	–3.0	–8.76	3.647	4.692	2.730
9	2.6	4.0	15.78	4.094	6.253	4.914
10	0.9	0.7	5.10	1.365	1.097	1.589
11	–5.3	–3.2	11.68	8.296	5.047	3.636
12	1.9	–3.6	–6.72	2.969	5.699	2.093
13	3.1	3.2	–19.12	4.899	4.983	5.956
14	–2.1	6.4	6.30	3.245	10.025	1.962
15	–2.3	3.3	12.82	3.653	5.139	3.993
16	–1.7	1.4	–0.58	2.709	2.181	0.182
17	–4.6	–7.4	13.06	7.262	11.570	4.067
18	–1.7	–3.7	–8.01	2.594	5.850	2.494
Mean	2.0	3.0	7.60	3.192	4.145	2.354

the *Y* output for design case 17. For cases 1—6, the maximum RE is 1.454 % (AE $9.000 \cdot 10^{-6}$ N) and occurs at the *X*-output for case 1.

All NNMs have smaller REs in the axial direction than the lateral one. For the considered models, the average axial REs are in the range of 2.3...3.6 %, and the lateral REs are in the range of 4.1...6.3 %.

Thus, it can be concluded that the smallest RE over the reduced variation interval occurs for the model NN-1024-512. As for the full variation inter-

Table 7. **Errors of force prediction for the NN-512 over the reduced interval**

No	AE			RE		
	Δf^x, 10^{-5} N	Δf^y, 10^{-5} N	Δf^z, 10^{-4} N	Δf^x, %	Δf^y, %	Δf^z, %
1	0.9	0.5	−1.87	1.485	0.771	0.582
2	0.7	1.8	−2.72	1.042	2.816	0.847
3	0.7	0.4	1.36	1.098	0.645	0.424
4	0.7	0.2	0.21	1.028	0.259	0.067
5	0.6	0.7	−2.12	0.987	1.064	0.660
6	0.7	0.6	−1.38	1.105	0.951	0.431
7	−3.4	−3.7	11.06	5.266	5.779	3.444
8	−3.1	2.8	−14.25	4.919	4.348	4.439
9	−3.9	6.3	7.36	6.107	9.931	2.291
10	−4.2	4.8	−0.87	6.511	7.475	0.271
11	−7.3	−2.6	15.04	11.387	4.142	4.683
12	−4.9	3.4	−14.06	7.657	5.313	4.380
13	4.0	4.6	−25.42	6.213	7.190	7.915
14	2.7	−1.6	−11.44	4.202	2.548	3.494
15	−4.7	4.2	−7.07	7.401	6.500	2.202
16	−4.3	3.8	−13.04	6.665	5.919	4.062
17	−9.0	−4.7	15.90	14.139	7.404	4.953
18	−3.3	−2.6	−11.39	5.158	3.995	3.549
Mean	3.0	3.0	8.70	5.132	4.281	2.705

Table 8. **Errors of force prediction for the NN-1024 over the reduced interval**

No	AE			RE		
	Δf^x, 10^{-5} N	Δf^y, 10^{-5} N	Δf^z, 10^{-4} N	Δf^x, %	Δf^y, %	Δf^z, %
1	0.9	0.4	−1.11	1.357	0.610	0.344
2	0.6	1.0	−1.77	0.938	1.488	0.551
3	−0.2	0.3	−0.40	0.266	0.504	0.124
4	−0.2	0.3	0.23	0.267	0.424	0.071
5	−0.2	0.7	−1.29	0.373	1.162	0.402
6	−0.2	0.4	−0.77	0.863	0.557	0.239
7	2.2	−1.3	3.97	3.378	1.977	1.238
8	−0.8	−2.8	−5.73	1.318	4.445	1.786
9	−1.0	1.3	13.82	1.616	1.982	4.304
10	−1.9	−2.0	9.42	3.011	3.178	2.934
11	−5.7	−3.8	12.97	8.893	5.910	4.040
12	−1.2	−2.9	3.36	1.812	4.503	1.046
13	1.8	1.2	−9.45	2.764	1.903	2.944
14	2.0	1.9	−2.88	3.152	2.973	0.896
15	−2.9	4.2	11.37	4.468	6.640	3.541
16	−2.5	3.6	−1.66	3.984	5.618	0.516
17	−2.5	−9.3	−10.40	3.933	14.599	3.240
18	−0.8	−3.3	−3.50	1.204	5.172	1.089
Mean	2.0	2.0	5.20	2.422	3.536	1.628

Table 9. **Errors of force prediction for the NN-1024-512 over the reduced interval**

No	AE			RE		
	Δf^x, 10^{-5} N	Δf^y, 10^{-5} N	Δf^z, 10^{-4} N	Δf^x, %	Δf^y, %	Δf^z, %
1	0.9	–0.3	1.55	1.454	0.412	0.483
2	–0.6	0.9	1.60	0.983	1.420	0.498
3	–0.4	–0.2	1.96	0.620	0.346	0.612
4	–0.1	–0.2	1.33	0.080	0.266	0.415
5	–0.2	–0.6	1.33	0.388	0.921	0.415
6	0.4	–0.3	1.42	0.619	0.509	0.443
7	–3.2	–1.9	5.93	4.957	2.913	1.848
8	–1.1	2.1	–2.96	1.660	3.328	0.923
9	1.5	3.3	9.13	2.391	5.100	2.845
10	0.8	0.7	4.92	1.318	1.058	1.534
11	3.5	2.6	11.68	5.529	4.003	3.636
12	–1.5	–1.7	–6.72	2.340	2.644	2.093
13	2.3	2.0	–6.69	3.667	3.108	2.082
14	1.4	2.5	3.05	2.161	3.880	0.951
15	–2.0	3.3	–4.39	3.203	5.139	1.366
16	–1.7	1.4	–0.58	2.645	2.181	0.182
17	3.2	–7.4	7.88	4.974	11.570	2.453
18	1.2	–3.7	–3.68	1.952	5.850	1.145
Mean	1.0	2.0	4.30	2.275	3.036	1.329

Table 10. **Time for the force determination using NNMs and CPBM**

No	Time for the force determination (sec)			
	NN-512	NN-1024	NN-1024-512	CPBM
1	6.350	6.305	6.291	17.660
2	6.084	6.492	6.085	17.514
3	12.584	12.306	12.479	38.009
4	9.640	10.532	10.037	27.443
5	9.796	9.773	9.606	28.019
6	9.526	9.568	9.626	28.003
7	6.053	6.221	6.103	11.840
8	6.193	6.139	6.168	11.505
9	12.131	12.150	12.543	26.556
10	9.586	9.718	9.651	15.862
11	9.690	9.807	9.652	20.317
12	9.640	9.572	9.734	15.768
13	6.267	6.390	6.108	11.827
14	6.347	6.395	6.333	11.513
15	12.221	12.310	12.533	26.321
16	9.664	10.796	14.444	15.938
17	11.050	11.536	11.189	19.715
18	11.043	11.239	11.010	16.088
Mean	9.104	9.292	9.422	19.994

val, all models coped with case 17 worst of all. As for the cases where the non-variable input parameters are nominal (1...6), the neural networks show significantly lower values of the maximum error in comparison with cases 7...18. In general, it can be said that the trends for the full variation interval are the same for the reduced interval, but the errors are noticeably smaller for the latter case.

For the considered models, the average axial RE over the reduced interval lies within the range of 1.3...2.7 %, and the lateral RE is within the range of 3.0...5.1 %.

The obtained results allow us to conclude that the proposed neural network models can predict the force impact of the IT plume on an SDO. For most of the considered cases, the errors of the force determination do not exceed 5 %. But even for cases where the relative error is higher than this value, the absolute error remains negligible. This fact suggests that such errors are insignificant in practice. Further improvement can be made to minimize errors for conditions such as in case 17. Although this case turns out to be the most difficult for all neural network configurations, it shows a tendency for the error to go down as the number of neurons in hidden layers increases.

2.7. ***Model performance analysis.*** To analyze the performance, we compare the time required to de-

termine the force using the NNMs and previously proposed approaches. As already noted in the introduction, the method of force determination based on the central projection of the target is considered to be the most effective so far [11, 12]. Therefore, this method was used for comparison. The time intervals for determining the force using the NNMs and the central projection-based method (CPBM) for various cases are presented in Table 10.

As can be seen from Table 10, the NNMs determine the force much faster in comparison with CPBM. For the considered cases, the NNMs require, on average, more than 2 times less time than CPBM. For case 3, the NSMs are 3 times faster than the CPBM. Within each of the considered cases, the time for determining the force by each of the three NNMs differs insignificantly.

Finally, it should be noted that despite the fact that the efficiency of the proposed approach is illustrated in the example of a cylindrical SDO, it can also be applied to other objects, taking into account the specifics of preparing the corresponding dataset for training an NNM.

CONCLUSION

The proposed approach shows the possibility of using deep learning methods to solve the problem of determining the force impact of the IT plume on the SDO. The influence of the configuration of the network model, as well as the relative position and orientation of the SDO, on the errors of the force determination is studied. The proposed models make it possible to determine the force much faster in comparison with the methods used before, which allows us to talk about prospects for using them both for spacecraft algorithms and mathematical simulation of space debris removal missions. Future research in this direction may investigate the efficiency of convolutional neural networks to determine the force impact from SDO images in orbit.

REFERENCES

1. Alpatov A. P., Cichocki F., Fokov A. A., Khoroshylov S. V., Merino M., Zakrzhevskii A. E. (2015). *Algorithm for determination of force transmitted by plume of ion thruster to orbital object using photo camera*. 66th Int. Astronautical Congress, Jerusalem, Israel, 2239—2247.
2. Alpatov A. P., Zakrzhevskii A. E., Fokov A. A., Khoroshylov S. V. (2015). Determination of optimal position of ion-beam shepherd in relation to space debris object. *Technical Mechanics*, № 2, 37—48.
3. Bombardelli C., Peláez J. (2011). Ion beam shepherd for contactless space debris removal. *JGCD*, **34**, № 3, 916—920. doi:10.2514//1.51832
4. Bombardelli C., Urrutxua H., Merino M., Ahedo E., Pelaez J. (2012). Relative dynamics and control of an ion beam shepherd satellite. *Spaceflight mechanics*, **143**, 2145—2158
5. Cichocki F., Merino M., Ahedo E. (2015). Collisionless plasma thruster plume expansion model. *Plasma Sources Sci. and Technol.*, **24**, № 3, 83—95.
6. Cybenko G. (1989). Approximation by superpositions of a sigmoidal function. *Mathematics of Control, Signals, and Systems*, **2**, № 4, 303—314. doi:10.1007//BF02551274.
7. Dron' M., Golubek A., Dubovik L., Dreus A., Heti K. (2019). Analysis of ballistic aspects in the combined method for removing space objects from the near Earth orbits. *Eastern-European J. Enterprise Technol.*, **2** (5 (98)), 49—54.
8. Fokov A. A., Khoroshilov S. V. (2016). Validation of simplified method for calculation of transmitted force from plume of electric thruster to orbital object. *Aviatsionno-kosmicheskaya tekhnika i tekhnologiya*, № 2, 55—66.
9. Golubek A., Dron' M., Dubovik L., Dreus A., Kulyk O., Khorolskiy P. (2020). Development of the combined method to de-orbit space objects using an electric rocket propulsion system. *Eastern-European J. Enterprise Technologies*, **4** (5 (106)), 78—87.
10. Hornik K. (1991). Approximation capabilities of multilayer feedforward networks. *Neural Networks*, **4**, № 2, 251—257. doi: 10.1016//0893-6080(91)90009-T.
11. Khoroshylov S. V. (2012). Relative control of an ion beam shepherd satellite in eccentric orbits. *Acta Astronautica*, № 76, 89—98.
12. Khoroshylov S. V. (2018). Relative motion control system of spacecraft for contactless space debris removal. *Nauka innov.*, 14, № 4, 5—16.

13. Khoroshylov S. V., Redka M. O. (2021). Deep learning for space guidance, navigation, and control. *Space Science and Technology*, 27, № 6 (133), 38—52.
14. Liou J.-C, Anilkumar A. K., Virgili B., Hanada T., Krag H., Lewis H. et al. (2013). *Stability of the future leo environment — an IAADC comparison study*. Proc. of the 6th European Conf. on Space Debris, 723. URL: https://conference.sdo.esoc.esa.int/proceedings/sdc6/paper/199 (Last accessed: 06.05.2022).
15. Mitchell T. (1997). *Machine Learning*. New York, NY: McGraw-Hill.
16. Phipps C. R., Reilly J. P. (1997). ORION: Clearing Near-Earth Space Debris in Two Years Using a 30-kW Repetitively-Pulsed Laser. *SPIE Proc. Int. Soc. Opt. Engineering*, 728—731.
17. Pierson H., Gashler M. (2017). Deep learning in robotics: a review of recent research. *Adv. Robotics*, 31, № 16, 821—835.
18. Takeichi N. (2006). Practical operation strategy for deorbit of an electrodynamic tethered system. *J. Spacecraft and Rockets*, **43**, № 6, 1283—1288. doi:10.2514//1.19635.

Стаття надійшла до редакції *06.05.2022* *Received 06.05.2022*
Після доопрацювання *02.06.2022* *Revised 02.06.2022*
Прийнято до друку *25.06.2022* *Accepted 25.06.2022*

М. О. Редька, аспірант
E-mail: mix5236@ukr.net
С. В. Хорошилов, пров. наук. співроб., д-р техн. наук, проф.
ORCID.org/0000-0001-7648-4791
E-mail: skh@ukr.net

Інститут технічної механіки Національної академії наук України
і Державного космічного агентства України
вул. Лешко-Попеля 15, Дніпро, Україна, 49005

ВИЗНАЧЕННЯ СИЛОВОГО ВПЛИВУ ФАКЕЛА ІОННОГО ДВИГУНА НА ОРБІТАЛЬНИЙ ОБ'ЄКТ ЗА ДОПОМОГОЮ ГЛИБИННОГО НАВЧАННЯ

Предметом дослідження у статі є процес створення нейромережевої моделі (НММ) для визначення силового впливу факелу електрореактивного двигуна (ЕРД) на орбітальний об'єкт під час безконтактного видалення космічного сміття.

Мета роботи — розробка НММ та дослідження впливу різних чинників на точність визначення сили, що передається потоком іонів ЕРД до об'єкта космічного сміття (ОКС).

Задачі: визначення структур НММ; формування набору даних для навчання та валідації НММ за допомогою сформованого набору даних; дослідження впливу структури моделі та параметрів оптимізатора на точність визначення сили. Використано методи фізики плазми, комп'ютерного моделювання, глибокого навчання, оптимізації із використанням вдосконаленого варіанта стохастичного градієнтного спуску.

Отримано такі **результати.** Розроблено три НММ, які відрізняються кількістю прихованих шарів та нейронів у прихованих шарах. Для навчання та валідації НММ з використанням автоподібного опису поширення іонів плазми згенеровано набір даних для ОКС, який апроксимовано циліндром. Набір даних отримано для різних відносних положень та орієнтацій об'єкта у процесі його відводу з орбіти. З використанням цього набору даних було виконано оптимізацію параметрів НММ за допомогою методу навчання із вчителем. Обрано оптимізатор та його параметри, які забезпечують найменшу похибку на етапі валідації результатів навчання. Визначено особливості впливу відносного положення та орієнтації ОКС, а також архітектури НММ на точність визначення сили.

Висновки. Показано можливість застосування методів глибинного навчання для вирішення задачі визначення сили впливу факела ЕРД на ОКС. Запропоновані моделі дозволяють забезпечити точність визначення силового впливу, достатню для вирішення розглянутого класу задач. При цьому НММ дає можливість отримувати результати значно швидше у порівнянні із методами, які використовувалися раніше, що робить їх перспективними для використання як для космічних апаратів, так і для математичного моделювання місій з видалення космічного сміття.

Ключові слова: електрореактивний двигун, об'єкт космічного сміття, сила що передається, нейромережева модель, глибинне навчання.